Struct Multidisc Optim (2014) 49:595–608
DOI 10.1007/s00158-013-0994-6

RESEARCH PAPER

Topology optimization of micro-structure for composites applying a decoupling multi-scale analysis

Junji Kato · Daishun Yachi · Kenjiro Terada · Takashi Kyoya

Received: 29 December 2012 / Revised: 30 July 2013 / Accepted: 25 August 2013 / Published online: 13 September 2013

Abstract The present study proposes topology optimization of a micro-structure for composites considering the macro-scopic structural response, applying a decoupling multi-scale analysis based on a homogenization approach. In this study, it is assumed that topology of macro-structure is unchanged and that topology of micro-structure is unique over the macro-structure. The stiffness of the macro-structure is maximized with a prescribed material volume of constituents under linear elastic regime. A gradient-based optimization strategy is applied and an analytical sensitivity approach based on *numerical material tests* is introduced. It was verified from a series of numerical examples that the proposed method has great potential for advanced material design.

Keywords Topology optimization · Decoupling multi-scale analysis · Micro-structures · Homogenization

1 Introduction

It is well known that the mechanical behavior of a composite material mainly depends on the geometric properties of the micro-structure, such as material distribution, shape or size of the material, and that the dependency will be remarkably increased in the non-linear regime in which material reaches fracture. It is becoming known that non-linear material behavior always closely relates to its micro-structure, for instance, in order to improve strength or toughness of a metallic material, crystal micro-structure enabling improvement of strength or toughness will be surveyed, and in order to improve energy-absorption capacity or wear resistance of synthetic rubber, micro-composition is investigated. It is said that what these composites have in common is that it will be possible to maximize the mechanical performance of a macro-structure, if 'types or kinds of materials to be mixed or the combinations thereof' are optimized and 'the geometric properties of micro-structure' are optimized.

As production technologies enabling control of material properties of micro-structure will be realized in the near future, this study proposes a method to maximize structural performance of macro-structure by optimizing the material distribution, topology in this study, in the micro-structure.

So far, study on topology optimization most often has been mainly developed for topology of macro-structure. With regard to the preceding studies on topology optimization of the micro-structure, for example, Sigmund (1994) proposes a method, named 'inverse-homogenization method', to determine topology of micro-structure that enables exhibiting stiffness equivalent to the prescribed material stiffness $\mathbb{C}^{\mathrm{H}}$. Sigmund and Torquato (1997) introduce a method, as its application, to determine topology of micro-structure that enables exhibiting a thermal expansion coefficient equivalent to the prescribed thermal expansion coefficient, and Larsen et al. (1997) also introduce topology of micro-structure able to exhibit negative Poisson's ratio. Amstutz et al. (2010) also propose an algorithm for optimization of micro-structures based on an exact formula for the topological derivative of the macroscopic elasticity tensor and a level set domain representation, where maximization of shear modulus and maximization/minimization

J. Kato (✉) · K. Terada
International Research Institute of Disaster Science,
Tohoku University 6-6, Aoba, Aramaki, Aoba-ku,
SENDAI 980-8579, Japan
e-mail: jkato@civil.tohoku.ac.jp

D. Yachi T. Kyoya
Mechanics of Materials Laboratory, Tohoku University 6-6,
Aoba, Aramaki, Aoba-ku, SENDAI 980-8579, Japan

of Poisson's ratio are described. However, these prominant studies focus on the micro-structure only, that is, governing equations consisting of a micro-scale boundary value problem (BVP) only, and do not basically consider behavior of macro-structure.

For the optimization problem dealing with both micro- and macro-structures, several methodologies have been developed. For example, Rodrigues et al. (2002) propose a hierarchical approach to optimize topologies of the micro- and macro-structure simultaneously, by considering behaviors of both structures. Niu et al. (2009) optimize topologies of both micro- and macro-structures for maximizing fundamental frequency based on the general homogenization theory, where topology of microstructure is assumed to be unique over the macro-structure. Su and Liu (2010) also propose an optimal micro-structure design considering the influence of macro-structural behavior based on the couple-stress theory. However, these applications are limited to linearly elastic structural problems although they are easy to implement.

In the meanwhile it is necessary to introduce a multi-scale analysis based on the homogenization method in order to solve the above-mentioned micro-macro coupling BVP. With regard to multi-scale analysis based on the homogenization method, many studies have been reported, and various analytical methods considering materially and/or geometrically nonlinear mechanical behavior have been proposed by, for example, Feyel and Chaboche (2000), Smit et al. (1998), Terada and Kikuchi (2001), Wieckowski (2000), and Zheng et al. (2000). As those methods solve all micro- and macro-scale BVPs simultaneously by reciprocal exchange in order to achieve higher precision on a micro-macro two-scale BVP, they are considered theoretically established and reliable. However, those analytical approaches are rarely applied to actual designing because they are theoretically difficult to understand and the computational costs are enormous.

The reason for it is briefly described as follows. Firstly, the macroscopic constitutive equation is an implicit function of the solutions of the micro-scale BVP and, thus, the micro-scale BVP indirectly represents the macroscopic material response. That is, it is not until the micro-scale equilibrated stress is determined that the macroscopic stress can be calculated. Therefore, if the two-scale coupling analysis is performed by the finite element method, the micro-scale BVP must be associated with an integration point located in a macro-scale finite element model and solved for the micro-scale equilibrated stress to evaluate the macro-scale stress by the averaging relation (1) introduced later, which must satisfy the macro-scale BVP at the same time. In particular, when an implicit and incremental solution method with a Newton–Raphson type iterative procedure is employed to solve the two- scale BVP, the micro-scale BVP is to be solved in every iteration to attain the macro-scale equilibrium state at every loading step. This type of solution scheme, i.e. the micro–macro coupling scheme, requires a significant amount of computational cost.

Taking this problem into account, (Terada et al. 2008, 2013; Watanabe and Terada 2010) propose a new method called *decoupling multi-scale analysis* to solve the micro-macro two-scale BVP by decoupling. This method is intended to reduce the computational costs by introducing an approximate approach called *numerical material tests* (NMTs), for the problems including numerically expensive calculations such as micro-macro two-scale BVPs with material and/or geometrical nonlinearity. Furthermore, as this approach is intended to solve a micro-scale BVP and a macro–scale BVP independently, this is a theoretcally-clear-approximate approach, and is superior in general-purpose use, because the method is applicable to various materials using the same framework. The details including the necessity and numerical accuracy of the decoupling multi-scale analysis compared to the micro-macro coupling multi-scale analysis are exclusively discussed in Watanabe and Terada (2010). Taking these characteristics into account, the decoupling of micro- and macro-scale BVPs is "indispensable" for applying the two-scale approach based on homogenization to various nonlinear structural problems encountered in practice.

As our final goal is to develop an optimization scheme for material designs considering materially and/or geometrically nonlinear structural behavior, this study applies the decoupling multi-scale analysis for optimization problems, specifically topology optimization of micro-structure considering the structural response of macro-scale structural analysis. However, as the present study stands only at the basic stage of introduction of the decoupling multi-scale analysis to optimization problems, this paper handles only topology optimization of micro-structure to maximize stiffness (to minimize compliance) of the macro-structure on the assumption of simply applying a two-dimensional plane strain problem in a linear elastic regime. Extension of our method to more realistic and complex nonlinear structural problems will be challenged in our next step. In that sense, the present paper is placed at the introductory material for the decoupling multiscale topology optimization considering nonlinear material models. Of course, for the micro–macro two–scale BVPs under an assumption of linear elasticity, no distinct advantage and difference exists between the coupling and decoupling schemes in computational costs.

In this study, we try to determine an optimal unique topology of a micro-structure to maximize stiffness of a macro-structure with keeping the initial topology of the macro-structure as a range of feasibility for actual production. The reason for not changing the topology of the macro-structure is to consider actual design circumstances in which the topology of a macro-structure is to be fixed to almost one by various conditions, such as in designing tires of automobiles using a synthetic rubber.

In the following, outline of the decoupling multi-scale analysis is described first, and then material models used in this study and the process of formulating the optimization problem are described. With regard to the algorithm for optimization, we use the optimality criteria method (Patnaik et al. 1995), hereinafter shown as OC method, on the basis of the gradient-based method that is effective in numerical analysis. In this paper, an analytical method on the basis of the adjoint method is proposed as the derivation of sensitivity, and the process of formulation is explained. Finally, the optimization method proposed in this paper is verified by a series of numerical examples.

2 Decoupling multi-scale analysis based on homogenization approach

2.1 Outline

Decoupling multi-scale analysis (Terada et al. 2013; Watanabe and Terada 2010) differs from a general approach to solve both parts of a micro- and macro-two-scale BVP simultaneously by maintaining coupling, but to solve the same problem as two independent boundary value problems by decoupling the boundary value problems. First, with regard to the micro-scale BVP, we extract a periodic micro-structure called 'unit cell', identified based on the homogeneous method, and then simulate the material tests on the micro-structure, regarding it as a numerical experiment. Then, by converting the results of micro-analysis to the macro-material parameters, we regard the conversion as measuring the material response of the macro-structure. A series of processes to identify macro-material behavior through numerical analysis on a unit cell like this is called a 'numerical material test'. In this study, as we assume linearly elastic material, we calculate a macro-stress $\boldsymbol{\Sigma}$ from the micro-stress $\boldsymbol{\sigma}$ obtained from micro-analysis, and then convert it into macro-material stiffness $\mathbb{C}^{\mathrm{H}}$. Then, the macro-scale BVP is solved by directly using the macro-material stiffness.

In the meantime, conventional linear multi-scale analysis calculates macro-material stiffness $\mathbb{C}^{\mathrm{H}}$ by introducing characteristic displacement (generally expressed as $\boldsymbol{\chi}$) on the assumption that the prescribed macro–strain $\boldsymbol{E}$ given to the unit cell has a linear relation with fluctuation displacement. However, the decoupling multi-scale analysis neither needs existence of characteristic displacement nor the assumption between the prescribed strain and the fluctuation displacement. As the method identifies the macro-stiffness from results of the numerical material test on the unit cell, it differs theoretically from the conventional micro-macro coupling multi-scale analysis. In the following, decoupling multi-scale analysis for the linear elastic model is outlined. Refer to the literatures (Terada et al. 2013; Watanabe and Terada 2010) for details of the decoupling scheme applied for nonlinear structural problems.

2.2 Micro-scale BVPs

Macro-structure is defined as a homogeneous body with force equivalent to the non-homogeneous elastic body having periodic micro-structure in the state of force equilibrium. Here, force equilibrium means that macro-stress $\boldsymbol{\Sigma}$ at an arbitrary point $\boldsymbol{x}$ in a macro-structure depends on a periodic micro-structure (unit cell) characterizing non-homogeneity, and is obtained by average volume of micro-stress $\boldsymbol{\sigma}$ distributed in the unit cell as shown in the following equation,

$$\boldsymbol{\Sigma} = \frac{1}{|Y|} \int_Y \boldsymbol{\sigma} \, \mathrm{d}y = \langle \boldsymbol{\sigma} \rangle \, . \tag{1}$$

Here, Y means the periodic micro-structure field, and $\boldsymbol{y}$, called a micro-scale variable, shows a position vector of an arbitrary point in a micro-structure. Similarly, the relation between macro-strain $\boldsymbol{E}$ and micro-strain $\boldsymbol{\varepsilon}$ is shown as follows:

$$\boldsymbol{E} = \frac{1}{|Y|} \int_Y \boldsymbol{\varepsilon} \, \mathrm{d}y = \langle \boldsymbol{\varepsilon} \rangle \, . \tag{2}$$

Micro-strain $\boldsymbol{\varepsilon}$ in (2) is defined by micro-displacement field $\boldsymbol{w}(\boldsymbol{x}, \boldsymbol{y})$ in a unit cell as follows:

$$\boldsymbol{\varepsilon} = \nabla_y^{\mathrm{sym}} w, \tag{3}$$

where $\boldsymbol{w}$ is assumed to be divided into two segments as shown in (4): (i) $\boldsymbol{E} \cdot \boldsymbol{y}$, a term distributed linearly in proportionate to macro-strain, and (ii) $\boldsymbol{u}^*$, fluctuation displacement which shows a gap from the linear distribution caused by the linear displacement field and heterogeneity,

$$\boldsymbol{w} = \boldsymbol{E}\,\boldsymbol{y} + \boldsymbol{u}^*. \tag{4}$$

Here, as usual in the computational homogenization, the fluctuation displacement $\boldsymbol{u}^*$ is restricted to be periodic on the boundary ∂Y of the unit cell, so that

$$\boldsymbol{u}^*|_{\partial Y^{[k]}} = \boldsymbol{u}^*|_{\partial Y^{[-k]}}, \quad \text{for } k = 1, 2 \quad \text{on } \partial Y. \tag{5}$$

As shown in Fig. 1, if the unit cell is a rectangular parallelepiped and its boundary is placed parallel to the

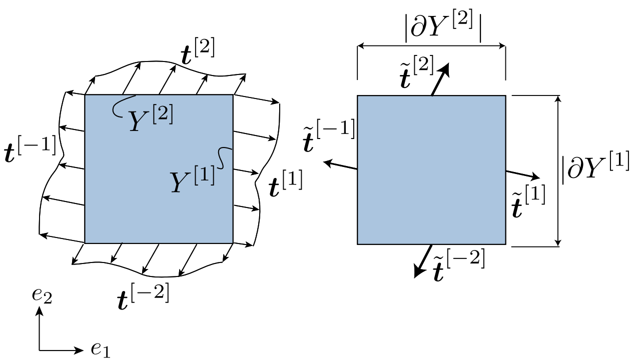

Fig. 1 Traction force vector $\boldsymbol{t}$ of a unit cell and macro-stress vector $\tilde{\boldsymbol{t}}$

coordinate axis, $\partial Y^{[k]}$ is a boundary which is parallel with $Y^{[k]}$ line, i.e., the boundary on which the orthonormal basis vector e_k, is to be the normal vector. From the periodicity of the fluctuation displacement, the following restriction is obtained for the actual displacement:

$$\boldsymbol{w}^{[k]} - \boldsymbol{w}^{[-k]} = \boldsymbol{E}\boldsymbol{L}^{[k]}. \tag{6}$$

In other words, this is a formula for constraint with respect to the relative displacement vector between boundary sides of periodicity to be coupled. For simplicity, we set as $\boldsymbol{w}^{[k]} := \boldsymbol{w}|_{\partial Y^{[k]}}$. Also, $\boldsymbol{L}^{[k]}$ is called a side vector of a unit cell that couples corresponding material points on a pair of boundaries in e_k-axial direction of a rectangular unit cell,

$$\boldsymbol{L}^{[k]} := \boldsymbol{Y}|_{\partial Y^{[k]}} - \boldsymbol{Y}|_{\partial Y^{[k-1]}}. \tag{7}$$

The other periodic boundary condition of a unit cell is that micro-traction force vector $\boldsymbol{t}^{[\boldsymbol{n}]} = \boldsymbol{\sigma} \cdot \boldsymbol{n}$ on a boundary having a unit vector $\boldsymbol{n}$ is to be imposed anti-periodic condition on the boundary of the unit cell to be coupled,

$$\boldsymbol{t}^{[k]} + \boldsymbol{t}^{[-k]} = \boldsymbol{0}, \tag{8}$$

where we set $\boldsymbol{t}^{[\pm k]} := \boldsymbol{t}^{[\pm e_k]}$ for simplicity. By integrating and averaging the micro-traction force vector $\boldsymbol{t}$ on the periodic boundary at the boundary of the unit cell, the macro-stress vector $\tilde{\boldsymbol{t}}$ can be obtained as the following equation (see Figs. 1 and 2),

$$\begin{aligned} \tilde{\boldsymbol{t}}^{[k]} &= \boldsymbol{\Sigma} \cdot e_k \\ &= \frac{1}{|\partial Y^{[k]}|} \int_{\partial Y^{[k]}} \boldsymbol{\sigma} \cdot e_k \mathrm{d}y = \frac{1}{|\partial Y^{[k]}|} \int_{\partial Y^{[k]}} \boldsymbol{t}^{[k]} \mathrm{d}y. \end{aligned} \tag{9}$$

By an equation adding the micro-scale equilibrium equation along with the constitutive law for the linearly elastic materials with elastic moduli $\mathbb{C}$ to the abovementioned

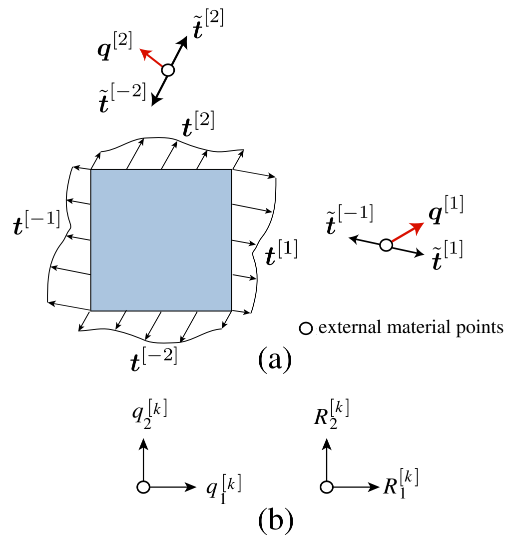

Fig. 2 **a** Concept of external material points having degrees of freedom for relative displacement vector and macro-stress vector, **b** degrees of freedom of relative displacement and the corresponding reaction force at an external material point in 2D

equation, a micro-scale BVP is defined. These equations are re-written after rearrangement as follows:

$$\left.\begin{aligned} &\nabla_y \cdot \boldsymbol{\sigma} = \boldsymbol{0} \\ &\boldsymbol{\sigma} = \mathbb{C} : \boldsymbol{\varepsilon} \\ &\boldsymbol{\varepsilon} = \nabla_y^{\mathrm{sym}} \boldsymbol{w} \\ &\boldsymbol{\Sigma} = \langle \boldsymbol{\sigma} \rangle \end{aligned}\right\} \quad \text{in} \quad Y, \tag{10}$$

$$\left.\begin{aligned} &\tilde{\boldsymbol{t}}^{[k]} = \frac{1}{|\partial Y^{[k]}|} \int_{\partial Y^{[k]}} \boldsymbol{t}^{[k]} \mathrm{d}y \\ &\boldsymbol{w}^{[k]} - \boldsymbol{w}^{[-k]} = \boldsymbol{E}\boldsymbol{L}^{[k]} \end{aligned}\right\} \quad \text{on} \quad \partial Y^{[k]}. \tag{11}$$

2.3 Extended system of a micro-scale BVP considering the external material points

Here, according to the literatures (Terada et al. 2013; Watanabe and Terada 2010), a formula employing a concept of external material point is introduced in contrast to boundary conditions about an aforementioned micro-scale BVP. First, a constraint condition to relative displacement around periodic boundary of a unit cell is written as follows:

$$\boldsymbol{w}^{[k]} - \boldsymbol{w}^{[-k]} = \boldsymbol{q}^{[k]}, \tag{12}$$

with

$$\boldsymbol{q}^{[k]} = \boldsymbol{E}\boldsymbol{L}^{[k]}, \tag{13}$$

where $\boldsymbol{q}^{[k]}$ means relative displacement vector between boundary sides of periodicity to be coupled. Also, as this is a two-dimensional problem, $\boldsymbol{L}^{[k]}$ can be written as follows:

$$\boldsymbol{L}^{[1]} = \left\{ l^{[1]} \ \ 0 \right\}^{\mathrm{T}} \quad \text{and} \quad \boldsymbol{L}^{[2]} = \left\{ 0 \ \ l^{[2]} \right\}^{\mathrm{T}}, \tag{14}$$

where $l^{[1]}, l^{[2]}$ show length of boundary sides of a rectangular parallel to e_1, e_2 axes respectively, namely, $l^{[1]} = |\partial Y^{[2]}|$ and $l^{[2]} = |\partial Y^{[1]}|$.

Terada et al. (2013) and Watanabe and Terada (2010), as shown in Fig. 2, placed arbitrary material points for each periodic boundary side $\partial Y^{[k]}$ $(k = 1, 2)$ to the direction of boundary normal lines respectively, and defined it as an 'external material point', and provided two degrees of freedom (DOFs) on each material point in parallel with e_1, e_2 axes, and allocated components of relative displacement vector $q^{[k]}$ to the DOFs of the external material points. Namely, (12) is a formula to control amount of relative displacement, which is calculated by the actual displacement vector of two points on the periodic boundaries to be coupled. In other words, the external material point is simply introduced as a control point for relative displacement and has no physical meanings. As even the coordinates of the external material points are arbitrary, the points are simply located near the corresponding boundaries as shown in Fig. 2.

Accordingly and consequently, as shown in (13), in order to provide arbitrary components of macro-strain $\boldsymbol{E}$ to the unit cell in the numerical material test, it is enough to control the components of relative displacement $q_j^{[k]}$ at the external material point (Fig. 3). Here, in order to make the meaning of (12) and (13) clear, the deformation of body and the corresponding macro-strin $\boldsymbol{E}$, together with relative displacements q are depicted in Fig. 4, where the parentheses on $\boldsymbol{E}$ indicates the tensile direction performed in the numerical material tests and $l^{[1]}$ and $l^{[2]}$ are assumed to be unit length for simplicity.

Now, if the relative displacement $q_j^{[k]}$ in (12) is given as a known vector, it just means that relative displacement $w_j^{[k]} - w_j^{[-k]}$ is given. The surface traction force vector $t_j^{[k]}$ on the boundary $\partial Y^{[k]}$ will turn out to be unknown. Consequently, the macro-stress vector $\tilde{t}_j^{[k]}$, the average of the surface traction force vector $t_j^{[k]}$ over the boundary $\partial Y^{[k]}$ will also turn out to be unknown.

However, if the reaction force of an external material point corresponding to known components of relative displacement vector $q_j^{[k]}$ is expressed as $R_j^{[k]}$, it is nothing but the definite integral of traction force vector $t_j^{[k]}$ linearly over the corresponding periodic boundary. Namely,

$$\boldsymbol{R}^{[k]} = \int_{\partial Y^{[k]}} \boldsymbol{t}^{[k]} \mathrm{d}y. \tag{15}$$

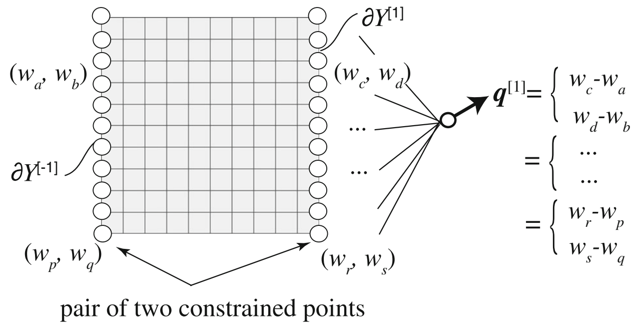

Fig. 3 Pair of constrained points and relative displacement vector

Consequently, in relation to (9), it is understood that the value of reaction of an external material point, (15), divided by a length of boundary line of the unit cell $|\partial Y^{[k]}|$ comes out to be an unknown macro-stress component Σ_{jk}. That is,

$$\Sigma_{jk} = \tilde{t}_j^{[k]} = \frac{R_j^{[k]}}{|\partial Y^{[k]}|}. \tag{16}$$

At this stage, when tensile numerical material tests are performed to three directions (11), (22), (12) independently, the components of the macro-material stiffness $\mathbb{C}^{\mathrm{H}}$ can be determined as follows:

$$\mathbb{C}^{\mathrm{H}}_{pqrs} = \Sigma^{(rs)}_{pq} \tag{17}$$

For implementation, (16) and (17) can be specifically expressed using the discrete formulation as follows:

$$\boldsymbol{\Sigma} = \begin{Bmatrix} \Sigma_{11} \\ \Sigma_{22} \\ \Sigma_{12} \end{Bmatrix} = \begin{Bmatrix} \tilde{t}_1^{[1]} \\ \tilde{t}_2^{[2]} \\ \tilde{t}_2^{[1]} = \tilde{t}_1^{[2]} \end{Bmatrix}, \tag{18}$$

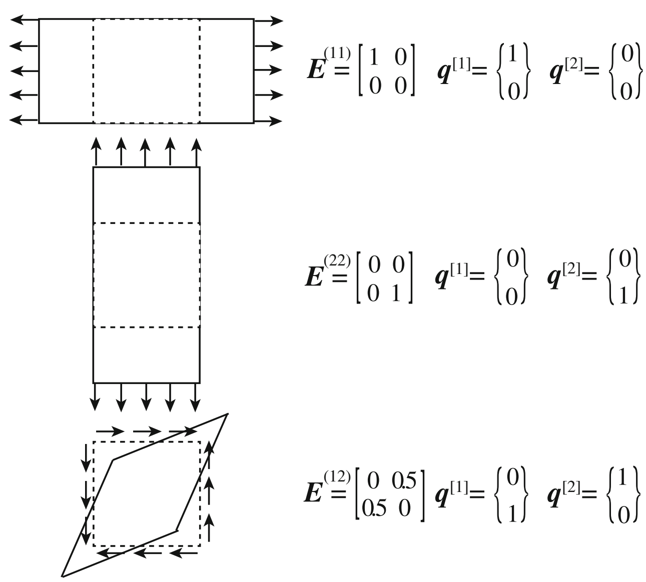

Fig. 4 Original and deformed homogenized bodies of unit cells (*left*) and its relation between macro-strain $\boldsymbol{E}$ and relative displacements $q^{[k]}(k = 1, 2)$ for 2D case, where $l^{[1]}$ and $l^{[2]}$ are assumed to be unit length for simplicity

and

$$\mathbb{C}^{\mathrm{H}} = \begin{bmatrix} \mathbb{C}_{11}^{\mathrm{H}} & \mathbb{C}_{12}^{\mathrm{H}} & \mathbb{C}_{13}^{\mathrm{H}} \\ \mathbb{C}_{12}^{\mathrm{H}} & \mathbb{C}_{22}^{\mathrm{H}} & \mathbb{C}_{23}^{\mathrm{H}} \\ \mathbb{C}_{13}^{\mathrm{H}} & \mathbb{C}_{23}^{\mathrm{H}} & \mathbb{C}_{33}^{\mathrm{H}} \end{bmatrix} = \begin{bmatrix} \Sigma_{11}^{(11)} & \Sigma_{11}^{(22)} & \Sigma_{11}^{(12)} \\ \Sigma_{22}^{(11)} & \Sigma_{22}^{(22)} & \Sigma_{22}^{(12)} \\ \Sigma_{12}^{(11)} & \Sigma_{12}^{(22)} & \Sigma_{12}^{(12)} \end{bmatrix}. \quad (19)$$

As a results, by using the macro-material stiffness $\mathbb{C}^{\mathrm{H}}$ given by the above numerical material test, it becomes possible to solve the macro-scale BVP.

This means resolving a micro-scale BVP including DOFs of newly introduced artificial external material points by providing relative displacement at the periodic boundary side to be coupled gives us the reaction force $R_j^{[k]}$ corresponding to the DOFs. This determines the macro-stress vector $\bar{t}_j^{[k]}$ by dividing by the length of the corresponding boundary. The macro-material physical properties necessary for macro structural analysis are to be obtained by directly using the macro-stress vector $\bar{t}_j^{[k]}$.

From this regard, if a micro-scale BVP is once resolved, it is possible to induce physical properties of macro-material from the response obtained, irrespective of material models to be used. That is to say, macro-material physical properties even having nonlinear behavior can be estimated or identified using a similar framework.

For the details of the finite element analysis of a unit cell with external material points, it is referred to Appendix.

3 Definition of design variable and material model for micro-structure

3.1 Definition of design variable

This section defines design variables for optimization and describes a micro-material model for composites. The material to be used in this study is a linearly elastic material excluding voids made of two-phase composite material consisting of two solid materials in micro-scale field, as shown in Fig. 5 (left, above). In this study, we use the finite element method to solve the micro-scale BVP, and define the design variable as volume fraction of constituent materials of each finite element in a unit cell,

$$s_i = \frac{r_i}{r_0}. \quad (20)$$

In the above formula, s_i means design variable, and is defined as a continuously varying function between $0 \leq s_i \leq 1$ similar to in the cases of the general topology optimization. Subscript $i\ (= 1, .., n_{\mathrm{ele}})$ means the i-th finite element and the subscript n_{ele} is the number of elements in a unit cell. r_0 and r_i show height of an arbitrary finite element and phase-2 material in a unit cell respectively, as shown in Fig. 5 (left, below).

Accordingly, in case $s_i = 0$, phase-1 occupies the element, and in contrast, in case $s_i = 1$, phase-2 occupies it. In the case of $0 < s_i < 1$, it is considered the mixture of both phases.

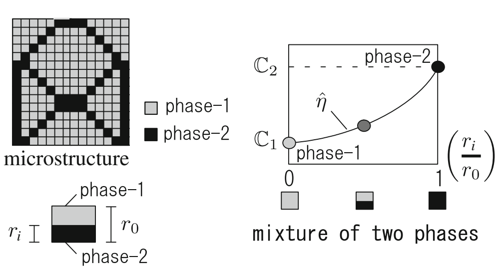

Fig. 5 Concept of two-phase material optimization

3.2 Material model for micro-structure

In this study as a material model for composite micro-structure, multiphase material model in Kato et al. (2009) assumed to be isotropic, linearly elastic material is used. The multiphase material model is what the concept of SIMP method (Zhou and Rozvany 1991) (Solid Isotropic Micro-structure with Penalization of intermediate densities), widely used to single porous material, is enlarged to composite and is the same as the multiple material model (Bendsøe and Sigmund 1999) in linear elastic case. The effective material stiffness is defined as follows:

$$\mathbb{C} = \left(1 - s_i^{\eta}\right)\mathbb{C}_1 + s_i^{\eta}\mathbb{C}_2. \quad (21)$$

Here, $\mathbb{C}$ is a material stiffness in the linear elastic regime, and is identical to that in (10). As clearly seen from the equation, it is understood that the material stiffness coefficient $\mathbb{C}$ explicitly depends on design variable s_i. $\mathbb{C}_1$ and $\mathbb{C}_2$ are known specific material stiffness of phase-1 and phase-2 respectively, and remain unchanged during the optimization. η is the power-law factor that does not guarantee the physical meaning.

4 Setting of optimization problem

Optimization problems are generally defined by objective function $f(\boldsymbol{s})$, equality constraint condition $h(\boldsymbol{s})$, and inequality constraint condition $g(\boldsymbol{s})$. The small bold italic letter $\boldsymbol{s}$ represents an array containing design variable s_i arranged in a row, i.e., it means design variable vector.

Hereafter, we present the process of formulation of an optimization problem handled in this study. As the objective is to maximize the stiffness of macro-structure, the following equations are formulated on the assumption that maximizing stiffness of the macro-structure is equivalent to minimizing the compliance. With regard to the constraint condition, we provide an equality constraint condition for the volume of phase-2 in the unit cell not to vary during optimization. In this optimization problem, as we set the only two kinds of material to exist, it means that the volume of phase-1 will not vary simultaneously as a whole unit cell. Furthermore, as the whole structure co-occupies one unit cell, it is self-evident that the volume of each individual material will not vary as a whole macro-structure. Then, the optimization problems expressed by the matrix form are shown as follows:

$$\min \ f(\boldsymbol{s}) = \boldsymbol{F}^{\mathrm{T}} \boldsymbol{d}, \tag{22}$$

$$h(\boldsymbol{s}) = \int_Y s_i \, \mathrm{d}Y - \hat{V} = 0, \tag{23}$$

$$s_{\mathrm{L}} \leq s_i \leq s_{\mathrm{U}} \qquad i = 1, \ldots, n_{\mathrm{s}}. \tag{24}$$

Here, $\boldsymbol{F}$ and $\boldsymbol{d}$ are external force vector and nodal displacement vector of the whole system of macro-structure, respectively. s_{L} and s_{U} are the lower and the upper bounds of design variables, n_{s} shows the number of design variables, which corresponds to the number of finite elements in the unit cell n_{ele} here. $\hat{V}$ is the prescribed total volume of phase-2 material in the unit cell.

As the optimization algorithm by the gradient-based method is used in this study, sensitivities of the objective function and constraint with respect to the design variable s_i, $\partial f / \partial s_i$ and $\partial h / \partial s_i$ respectively, should be obtained after resolving the two-scale BVP. By incorporating the thus-obtained sensitivity into the optimality criteria method, the optimized solution at that time is obtained. Then, the solution is subjected to repeated calculations until the solution is converged (Fig. 6). In the following section, derivation of sensitivity of objective function is explained. As the sensitivity of constraint with respect to the design variable is derived as the same approach as that of the general topology optimization, the explanation for it is eliminated in this paper.

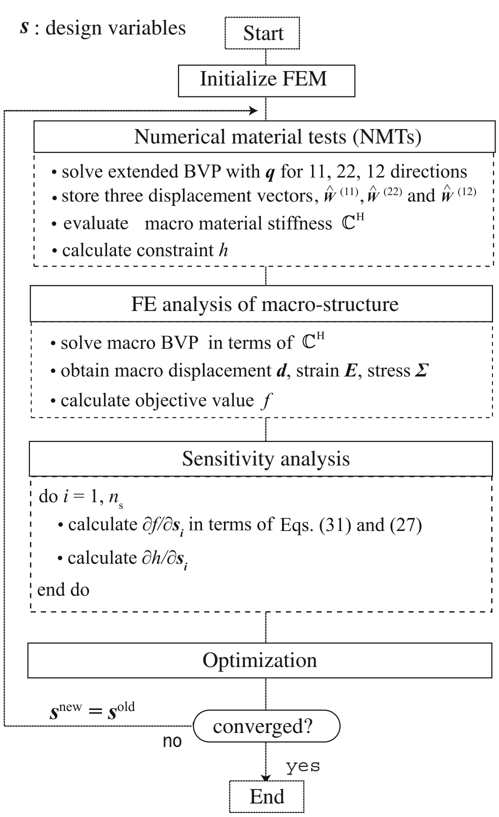

Fig. 6 Flowchart of optimization procedure for the proposed method

5 Sensitivity analysis

5.1 Sensitivity of objective function

In this section, the process to obtain sensitivity of objective function f with respect to design variable s_i is explained. Specifically, the sensitivity is derived by the adjoint method, more accurately, the analytical adjoint method. First, the objective function f is converted to equivalent objective function $\bar{f}$ with a constraint condition of discretized formulation of equilibrium equation $\boldsymbol{Kd} = \boldsymbol{F}$, $\boldsymbol{K}$ as global stiffness matrix of macro-structure,

$$\bar{f}(\boldsymbol{s}) = \boldsymbol{d}^{\mathrm{T}} \boldsymbol{K} \boldsymbol{d} - \tilde{\boldsymbol{d}}^{\mathrm{T}} (\boldsymbol{K}\boldsymbol{d} - \boldsymbol{F}), \tag{25}$$

where $\tilde{\boldsymbol{d}}$ is an adjoint vector. Next, the above (25) is differentiated by design variable s_i and arranged as follows:

$$\frac{\partial \bar{f}}{\partial s_i} = \left(\underbrace{\boldsymbol{d}^{\mathrm{T}} \boldsymbol{K}}_{\boldsymbol{F}^{\mathrm{T}}} - \tilde{\boldsymbol{d}}^{\mathrm{T}} \boldsymbol{K} \right) \frac{\partial \boldsymbol{d}}{\partial s_i} - \tilde{\boldsymbol{d}}^{\mathrm{T}} \frac{\partial \boldsymbol{K}}{\partial s_i} \boldsymbol{d}. \tag{26}$$

Then, it should be noticed that the adjoint vector $\tilde{\boldsymbol{d}}$ does not depend on design variable s_i, because the adjoint vector $\tilde{\boldsymbol{d}}$ is arbitrary. In this equation, the term unable to be obtained explicitly is a differential term regarding displacement $\partial \boldsymbol{d} / \partial s_i$. Then, when the adjoint vector $\tilde{\boldsymbol{d}}$ is placed as $\tilde{\boldsymbol{d}} = \boldsymbol{d}$ to make the amount in the parenthesis of the first term in the right side zero, the implicit differential term disappears. By rearranging (26) again, the equation is transformed to the form that is able to obtain a solution explicitely and easily, as shown in the first line of the following (27). Furthermore, by reversing the equation to the notation according to the finite element level, as shown in the second line, the sensitivity of the objective function can be easily obtained, if the derivative of macro-material stiffness matrix $\partial\mathbb{C}^{\mathrm{H}}/\partial s_i$ is calculated as,

$$\frac{\partial \bar{f}}{\partial s_i}\left(=\frac{\partial f}{\partial s_i}\right) = -\boldsymbol{d}^{\mathrm{T}}\frac{\partial \boldsymbol{K}}{\partial s_i}\boldsymbol{d} = -\int_{\Omega}\boldsymbol{E}^{\mathrm{T}}\frac{\partial\mathbb{C}^{\mathrm{H}}}{\partial s_i}\boldsymbol{E}\,\mathrm{d}\Omega, \tag{27}$$

where $\boldsymbol{E}$ denotes the macro strain obtained by macro-scale BVP, and not the given macro-strain used in numerical material tests. Thus, the macro-scale sensitivity can be separately obtained if the remaining term, $\partial\mathbb{C}^{\mathrm{H}}/\partial s_i$, is calculated. In the following section, we propose the derivation of the sensitivity, $\partial\mathbb{C}^{\mathrm{H}}/\partial s_i$, in an analytical formulation.

5.2 Derivation of sensitivity of macro-material stiffness tensor

Recalling the tensor formulation of (17), we transform its component into the following expression in terms of (1),

$$\begin{aligned}\mathbb{C}^{\mathrm{H}}_{pqrs} &= \Sigma^{(rs)}_{pq}\\ &= \frac{1}{|Y|}\int_Y \sigma_{pq}\left(\boldsymbol{\varepsilon}^{(rs)}\right)\mathrm{d}y\\ &= \frac{1}{|Y|}\int_Y \boldsymbol{\sigma}\left(\boldsymbol{\varepsilon}^{(rs)}\right):\boldsymbol{E}^{(pq)}\,\mathrm{d}y\\ &= \frac{1}{|Y|}\int_Y \mathbb{C}:\boldsymbol{\varepsilon}^{(rs)}:\left(\boldsymbol{\varepsilon}^{(pq)}-\boldsymbol{\varepsilon}^{*(pq)}\right)\mathrm{d}y\\ &= \frac{1}{|Y|}\int_Y \mathbb{C}:\boldsymbol{\varepsilon}^{(pq)}:\boldsymbol{\varepsilon}^{(rs)}\,\mathrm{d}y,\end{aligned} \tag{28}$$

where we rewrite the strain field of fluctuation as $\boldsymbol{\varepsilon}^* = \nabla^{\mathrm{sym}}_y\boldsymbol{u}^*$. In the fourth equilibrium, the relation $\boldsymbol{\varepsilon}^{(pq)} = \boldsymbol{E}^{(pq)}+\boldsymbol{\varepsilon}^{*(pq)}$ is employed and in the fifth equilibrium, the term with fluctuation strain $\boldsymbol{\varepsilon}^*$ is eliminated in terms of (33), where the fluctuation strain $\boldsymbol{\varepsilon}^*$ is used instead of the virtual fluctuation strain field $\delta\boldsymbol{\varepsilon}^*$ for its arbitrariness.

Differentiating (28) with respect to design variable s_i yields

$$\begin{aligned}\frac{\partial\mathbb{C}^{\mathrm{H}}_{pqrs}}{\partial s_i} &= \frac{1}{|Y|}\int_Y \frac{\partial\mathbb{C}}{\partial s_i}:\boldsymbol{\varepsilon}^{(pq)}:\boldsymbol{\varepsilon}^{(rs)}\,\mathrm{d}y\\ &+\frac{1}{|Y|}\int_Y \mathbb{C}:\frac{\partial\boldsymbol{\varepsilon}^{*(pq)}}{\partial s_i}:\left(\boldsymbol{E}^{(rs)}+\boldsymbol{\varepsilon}^{*(rs)}\right)\mathrm{d}y\\ &+\frac{1}{|Y|}\int_Y \mathbb{C}:\left(\boldsymbol{E}^{(pq)}+\boldsymbol{\varepsilon}^{*(pq)}\right):\frac{\partial\boldsymbol{\varepsilon}^{*(rs)}}{\partial s_i}\mathrm{d}y.\end{aligned} \tag{29}$$

Here, we replace the virtual strain field $\delta\boldsymbol{\varepsilon}^*$ in (33) by $\partial\boldsymbol{\varepsilon}^*/\partial s_i$ considering its arbitrariness and periodicity, and insert the modified equation (33) into (29). This procedure eliminates the second and third summations of (29), thus (29) is simply rewritten as follows:

$$\frac{\partial\mathbb{C}^{\mathrm{H}}_{pqrs}}{\partial s_i} = \frac{1}{|Y|}\int_Y \frac{\partial\mathbb{C}}{\partial s_i}:\boldsymbol{\varepsilon}^{(pq)}:\boldsymbol{\varepsilon}^{(rs)}\,\mathrm{d}y. \tag{30}$$

Finally, for implementation, the discretized formulation of (30) is written in the following expression:

$$\begin{aligned}\frac{\partial\mathbb{C}^{\mathrm{H}}_{\alpha\beta}}{\partial s_i} &= \frac{1}{|Y|}\int_Y \hat{w}^{\mathrm{e}\,\mathrm{T}}_{\alpha}\boldsymbol{B}^{\mathrm{T}}\frac{\partial\mathbb{C}}{\partial s_i}\boldsymbol{B}\hat{w}^{\mathrm{e}}_{\beta}\,\mathrm{d}y\\ \text{with}\quad \frac{\partial\mathbb{C}}{\partial s_i} &= \eta s_i^{\eta-1}\left(\mathbb{C}_2-\mathbb{C}_1\right),\end{aligned} \tag{31}$$

where $\hat{\boldsymbol{w}}^{\mathrm{e}}$ denotes the nodal micro-displacement vector of an element in a unit cell, and its discretization procedure is referred to Appendix. Although the symbols for the direction of the numerical material tests, i.e. (pq) and (rs), have been abbreviated in (31) for simplicity , they are still effective. As described in Appendix, the nodal displacement vector $\hat{\boldsymbol{w}}^{\mathrm{e}}$ is obtained as the result of the numerical material tests.

In the solution procedure, the global nodal displacement vector for each loading direction, i.e. $\hat{\boldsymbol{w}}^{(11)}$, $\hat{\boldsymbol{w}}^{(22)}$ and $\hat{\boldsymbol{w}}^{(12)}$, or the condensed version of the displacement, i.e. $\tilde{\boldsymbol{w}}^{(11)}$, $\tilde{\boldsymbol{w}}^{(22)}$ and $\tilde{\boldsymbol{w}}^{(12)}$ introduced in (40), should be stored in order to calculate each component of $\partial\mathbb{C}^{\mathrm{H}}_{\alpha\beta}/\partial s_i$, which is obtained from combination of the above three kinds of displacement vectors. For reference, the entire procedure of the proposed method is described in Fig. 3.

6 Verification of the proposed method by numerical examples

6.1 Common problems

In this section, the proposed method, topology optimization of micro-structure by decoupling multi-scale analysis, is verified using a series of numerical examples. The point to be cleared in this verification is whether or not this approach can obtain topology of micro-structure which characterizing the emechanical behavior of macro-structuref properly. For this purpose, it is designed to easily assess the examples of verification in the former half by providing basic uniform deformation to a simple macro-structure model constructed by a 4-node rectangular element in order to avoid difficulty in assessing the results of optimization. In the numerical examples in the latter half, comparative verification was performed among the macro-structures with increased number of finite elements and with conflicting geometric properties. In this verification, it should be noticed that any example of optimization is 'non-uniqueness' that means any solution for optimization is not unified. This means that mathematically plural solutions for optimization may exist for the same objective function. Therefore, it is possible for the same topology optimization problem to lead to a different solution due to different computers used, and both results are the optimum solutions. Obtaining a different topology in the same unit cell might be caused by minor errors in the numerical analysis, e.g., intrinsic faint errors in a computer or in calculation program; the phenomenon itself is numerically correct as introduced in Sigmund and Pettersson (1998).

This situation for the optimization solution not to be unified is caused by a 'uniform deformation' which occurs in a unit cell. Such deformation occurs when boundary conditions of a unit cell have periodicity and all the finite elements in a unit cell are provided with the same physical properties. A situation like this is often seen in the initial structure before starting the optimization calculation. At this time, when the sensitivity of the objective function $\partial f/\partial s_i$ (vector) is calculated, all the elements show the same value of sensitivity, and the contribution of each element to the objective function is assessed as equal. Accordingly, from the theoretical viewpoint, further optimization will not be calculated.

But, in this case, despite the existence of inevitable minor errors as mentioned above, we are able to continue the optimization calculation by tracing the minimal difference among elements of $\partial f/\partial s_i$. In such cases, the authors have confirmed through our experience that three scenarios will develop as follows: (a) topology remains unchanged, almost keeping the same initial stage, (b) topology disturbed by the abovementioned difference becomes disturbed and meaningless due to dependency on the initial value of design variable, characteristic of the gradient-based method, or (c) topology stagnates showing checkerboard pattern introduced in Diaz and Sigmund (1995) and Jog and Haber (1996).

In this study, as one of the countermeasures to avoid this problem, we employed the mesh-independent filter method proposed by Bendsøe and Sigmund (2003), Sigmund and Pettersson (1998), evaluated as the most effective, as follows:

$$\frac{\partial \tilde{f}}{\partial s_i} = \frac{1}{s_i \sum_{j=1}^{N} \hat{H}_j} \sum_{j=1}^{N} \hat{H}_j s_j \frac{\partial f}{\partial s_j}$$

$$\text{with} \qquad \hat{H}_j = r_{\min} - \mathrm{dist}(i, j). \tag{32}$$

In the above equation, $\mathrm{dist}(i, j)$ shows the center-to-center distance of ith and jth finite elements, $r_{\min}$, called a filter radius, determines a range of elements to be filtered.

In the numerical examples here, we tried to obtain the final topology with two phases distinguished as clearly as possible by using a filter with rather large radius $r_{\min}$ at the beginning of optimization to avoid locally stagnant topology and tuning the radius gradually smaller. In this study, the minimum value of $r_{\min}$ is set to be a slightly larger value than the center-to-center distance between adjacent elements to avoid numerical instability.

6.2 Case of a simple structure discretized with a 4-node rectangular element

This numerical example is to verify whether or not a reasonable topology is obtained when a macro-structure, modeled with a simple structure discretized with a 4-node rectangular element, is provided with a uniform deformation. The macro-structure of a square with a side of 100 mm is modeled using a plane strain element. The material used inside the micro-structure is assumed to be of two kinds (two-phase composite material consisting of two solid materials in micro-field) excluding voids. Here, the material stiffness of phase-2 (black) is set larger than that of phase-1 (white). All the material used is assumed to be a linearly elastic model. The material properties used are shown in Table 1. With regard to the power-law factor η, shown in (21), we used as $\eta = 5$ in every case.

The shape of the unit cell is set to as a square, and the length of a side is normalized and set to the unit length. Finite elements used were 8-node rectangular elements, and the number of elements was 400 (20 x 20). At the initial stage before optimization, we assumed that every element

Table 1 Material data

	Young's modulus (MPa)	Poisson's ratio
phase–1	10	0.3
phase–2	10000	0.3

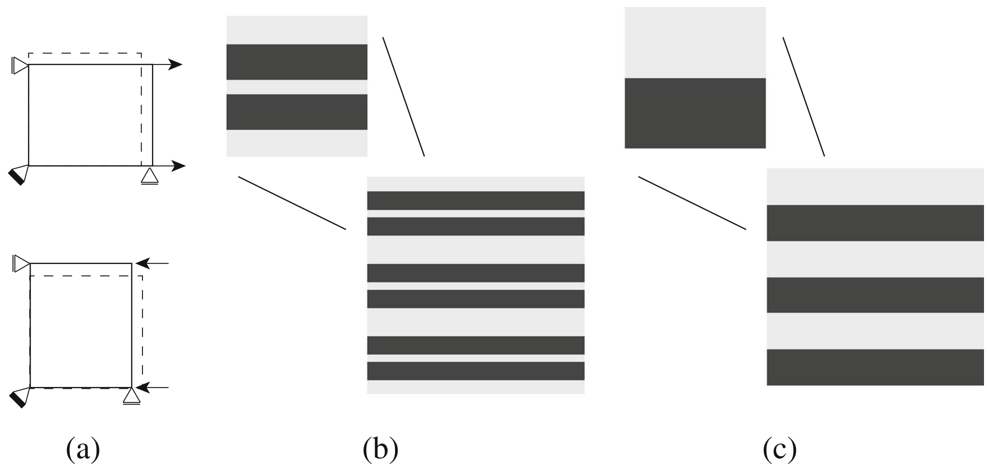

Fig. 7 **a** Conceptual diagrams of uniform tension/compression deformation of macro-structure, (**b**), (**c**) the optimized topology of micro-structure (a unit cell and its patch); **b** Case, the radius of a filter $r_{\min}$ is 0.051(the minimum value) until the number of optimization steps reaches 100 and thereafter the filter was eliminated, **c** $r_{\min}$ is reduced from 0.251 to 0.051 (the minimum value) by degrees

was included in each phase-1 and phase-2 by 50 % respectively. Thus, the initial value of the design variable was set to $s_i = 0.5$ in every element. The total volume of material included in the structure was set to remain unchanged during the optimization. In this connection, we used the same assumption for all the unit cells used in this paper.

Hereafter, results of optimization obtained in the numerical examples are explained. First, Fig. 7a shows a conceptual diagram of deformation provided to the macro-structure. We provided 10 % strain as uniaxial tensile or compression deformation. Figure 7b shows the result of optimization in a case that the radius of the filter $r_{\min}$ was set to be a slightly larger value (0.051) than the center-to-center distance (0.05) between adjacent elements until the number of optimization steps reached 100, and thereafter the filter was eliminated. On the other hand, Fig. 7c shows the results of optimization with a thicker layer of phase-2 than in the previous cases, because we reduced the radius of the filter gradually according to the increase of the number of optimization steps for longer distance initially set among 5 elements (initial $r_{\min} = 0.05 \times 5 +$ small value $0.01 = 0.251$). This is due to the problem of non-uniqueness, which confirmed that different topologies were obtained according to the setting of the filtering radius. As far as these two results are concerned, either exhibits the most suitable structure to increase stiffness for either direction tensile or compression.

Next, Fig. 8 shows the result of optimization when the macro-structure is subjected to a simple shear deformation. The topology obtained shows the material distribution with the inclination of 45 degrees from the horizontal line, which is the result we expected. In some cases, topology turned around 180 degrees with respect to e_2-axis, i.e. topology with the inclination of -45 degrees, was obtained. This result also introduces the non-uniqueness problem and the obtained both macro-material stiffness matrices $\mathbb{C}^{\mathrm{H}}$ are identical.

From the above examples, it is confirmed that the proposed method can determine a mechanically reasonable topology for behavior of a simple macro-structure.

6.3 Cases for various macro-structures

Considering the verification results in the previous section, the proposed method for several representative behaviors of macro-structure, including bending deformation, is to be verified in this section. In the following examples, we used a macro-structure with 8-node rectangular elements, and assumed plane strain condition.

Figure 9 shows the result of optimization when a uniform load of 1.0kN/mm was applied to a beam 200 mm long and 100 mm high. Figure 9 top shows the distribution of the horizontal stress σ_{xx} (MPa) with deformation and the middle shows the distribution of shear stress σ_{xy} (MPa). From Fig. 9 it is understood that the horizontal

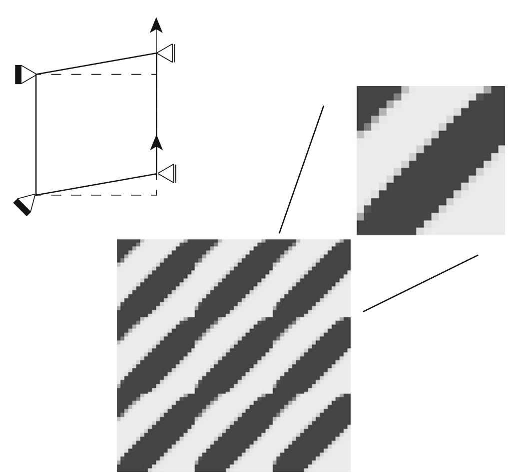

Fig. 8 Conceptual diagrams of uniform shear deformation of macro-structure and the optimized topology of micro-structure (unit cell and its patch)

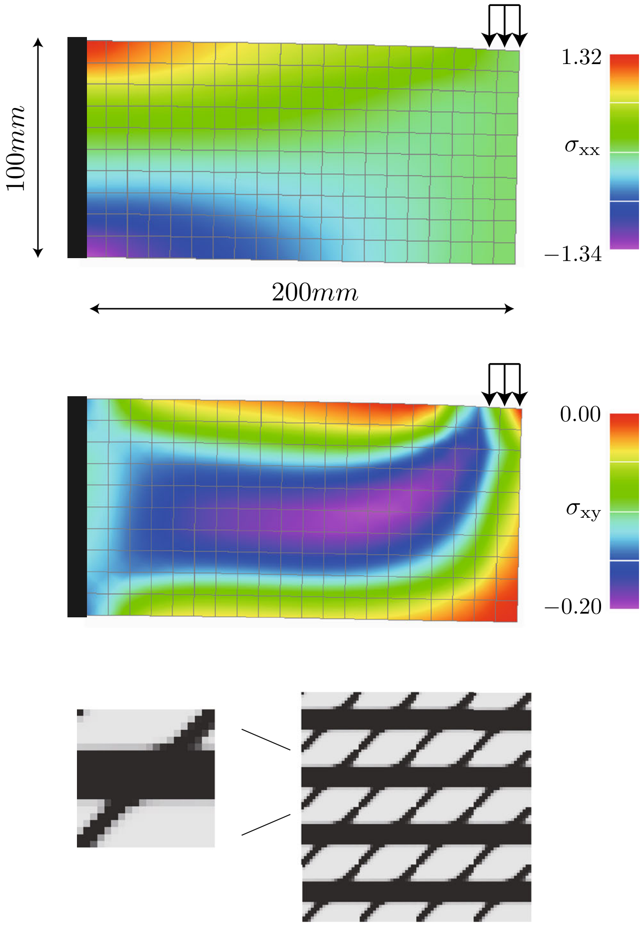

Fig. 9 Result of topology optimization of micro-structure in case of a macro-cantilever beam: deformation and horizontal stress σ_{xx} diagram (*top*), deformation and shear stress σ_{xy} diagram (middle), optimized micro-structure (*bottom*)

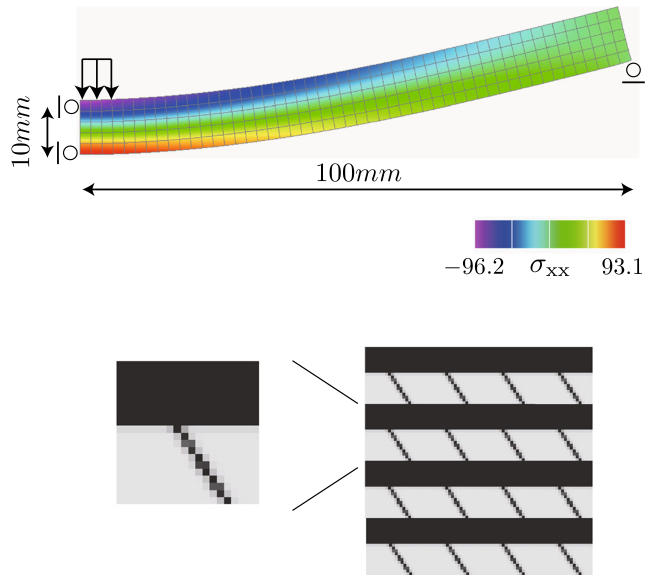

Fig. 10 Results of optimization of micro-structure in case of a macro-slender beam: deformation and horizontal stress σ_{xx} diagram (*top*) and optimized micro-structure (*bottom*)

stresses dominate at both the top and bottom ends on the left boundary of the beam, and shear stresses are shown to almost the whole area of the macro-structure, although the shear stresses are rather small compared to the maximum horizontal stress. The optimized micro-structure shows that topology with a thick layer of the phase-2 arranged horizontally as a reinforcement for horizontal stresses and diagonal reinforcement against shear stresses is obtained. From the above results, it is considered that the optimization structure is reasonable as concerns structural mechanics.

Figure 10 shows the result of optimization of a macro-structure that is modeled from a right half-section of a simple slender beam. In this example, a uniformly distributed load of 6.0kN/mm was applied on the upper surface of the beam. The upper diagram in Fig. 10 shows its deformation and horizontal stress distribution. As clearly noticed from the diagram, the macro-structure is a structure in which the horizontal stress dominates and large shear stress does not occur because of low beam height (Diagram of shear stress is omitted). As the result, the optimized micro-structure shows that most of the phase-2 material is arranged to the direction of the horizontal axis, and the topology shows slightly diagonal to reinforce against the shear stresses. Here, looking at deeper inside of Fig. 10, one may notice that the slightly diagonal thin layer in the obtained topology is one-node hinged layout. Although the obtained topology is structural reasonable as mentioned above, this kind of layout may be cured by using more advanced filter method such as *Morpho–logy–based black and white filter* developed by Sigmund (2007).

Figure 11 shows the results of optimization using a macro-structure of a deep beam under the same structural condition. As the stress distribution of the macro-structure considerably differs because of difference in height of a beam, this is to verify whether or not optimization of micro-structure properly recognizing the difference of stress distribution is obtained. Figure 11 left shows distribution of shear stress σ_{xy} (MPa), and Fig. 11 center shows distribution of vertical stress σ_{yy} (MPa). As the absolute value of horizontal stress is so small, a diagram of horizontal stress σ_{xx} is omitted. From the diagram it is understood that the distribution of shear stress dominates on the line connecting the loading points to the supporting point. With regard to the distribution of vertical stress, large compression stress occurs adjacent to a loading point and vertical supporting point, and especially at the vertical supporting point, large stress concentration exceeding -250 (MPa) is seen. As the result, topology reinforced by diagonal direction for

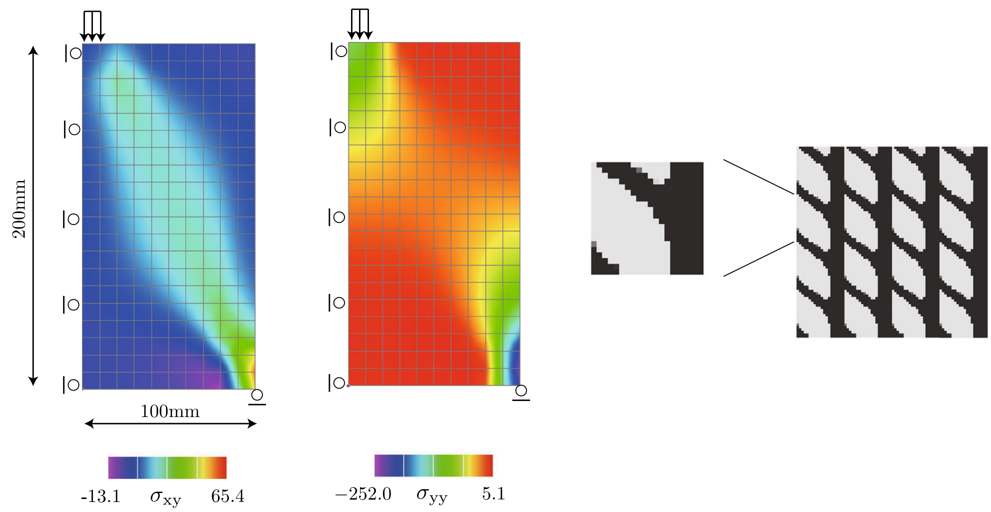

Fig. 11 Results of topology optimization of micro-structure in case of a macro-deep beam: shear stress σ_{xy} (*left*) and optimized micro-structure (*right*), vertical stress σ_{yy} (*middle*) and optimized micro-structure (*right*)

shear stress and upright direction for vertical stress appeared on the optimized micro-structure. Consequently, it is considered that the topology of micro-structure considering characteristics of macro-structure is obtained.

From all these optimization calculations, it is verified that the approach proposed in this study can optimize topology of a micro-structure by reflecting mechanical behavior of the macro-structure in the linear elastic regime.

6.4 Conclusion

The purpose of this study is to propose an approach to maximize the performance of macro-structure by optimizing the topology of micro-structure of composite material. In this study, an optimization method that is intended to maximize the stiffness of a macro-structure under the new framework of introducing decoupling multi-scale analysis into topology optimization is proposed, and the proposed method was verified through various numerical calculations.

Main results of this study are as follows:

- It was verified that the proposed method reflects the mechanical behavior of macro-structure with high fidelity and that the method optimizes topology of micro-structure by all the optimization examples.
- An analytical sensitivity approach was formulated considering both micro- and macroscopic structural response. In this methodology, no extra assumption is necessary which is concerned with the linear relation between micro- and macro–scale deformation defined by the characteristic displacement.
- In this paper, we implemented topology optimization of microstructure for the micro–macro two–scale BVPs under an assumption of linear elasticity. As mentioned in the Introduction, no distinct advantage and difference exists between the coupling and decoupling schemes in computational costs under the linear elastic regime. It is expected that this approach will be extended to non-linear structural problems in considering the essential effect of decoupling multi-scale analysis.

Acknowledgments This work was supported by MEXT KAKENHI Grant Numbers 23560561, 23656285. These supports are gratefully acknowledged.

Appendix: Finite element analysis for a unit cell with external material points

For preparation of the finite element analysis (FEA) for the micro-scale BVP, the spatial domain of the unit cell is discretized to generate its FE mesh. The principle of virtual work for micro-structure is formulated considering the first equation in (10) and anti-periodicity condition (8) with some mathematical rearrangement as follows:

$$\int_Y \delta\boldsymbol{\varepsilon}^* : \boldsymbol{\sigma}\,\mathrm{d}y = \int_Y \nabla_y^{\mathrm{sym}} \delta\boldsymbol{u}^* : \boldsymbol{\sigma}\,\mathrm{d}y = 0, \tag{33}$$

where $\delta\boldsymbol{u}^*$ and $\delta\boldsymbol{\varepsilon}^*$ denote the virtual fluctuation displacement field and its strain field satisfying the periodic condition, respectively. The virtual work expression (33) is discretized in the finite element sense assuming the following approximation:

$$\boldsymbol{w} = \sum_{\alpha=1}^{n_{\mathrm{node}}} N_\alpha \hat{w}_\alpha^{\mathrm{e}} \quad \text{or} \quad \boldsymbol{w} = \boldsymbol{N}\hat{\boldsymbol{w}}^{\mathrm{e}}, \tag{34}$$

$$\delta\boldsymbol{w} = \sum_{\alpha=1}^{n_{\mathrm{node}}} N_\alpha \delta\hat{w}_\alpha^{\mathrm{e}} \quad \text{or} \quad \delta\boldsymbol{w} = \boldsymbol{N}\delta\hat{\boldsymbol{w}}^{\mathrm{e}}, \tag{35}$$

$$\boldsymbol{\varepsilon} = \sum_{\alpha=1}^{n_{\mathrm{node}}} B_\alpha \hat{w}_\alpha^{\mathrm{e}} \quad \text{or} \quad \boldsymbol{\varepsilon} = \boldsymbol{B}\hat{\boldsymbol{w}}^{\mathrm{e}}, \tag{36}$$

$$\delta\boldsymbol{\varepsilon} = \sum_{\alpha=1}^{n_{\mathrm{node}}} B_\alpha \delta\hat{w}_\alpha^{\mathrm{e}} \quad \text{or} \quad \delta\boldsymbol{\varepsilon} = \boldsymbol{B}\hat{\boldsymbol{w}}^{\mathrm{e}}, \tag{37}$$

where $\boldsymbol{N}$ is the general shape function and $\boldsymbol{B}$ the B-operator, respectively. $\hat{\boldsymbol{w}}^{\mathrm{e}}$ indicates the nodal micro-displacement vector of an element in a unit cell. Furthermore, we similarly discretize $\delta\boldsymbol{u}^*$ and $\delta\boldsymbol{\varepsilon}^*$ as $\delta\boldsymbol{u}^* = \boldsymbol{N}\left(\delta\hat{\boldsymbol{d}}^{*\mathrm{e}}\right)$ and $\delta\boldsymbol{\varepsilon}^* = \boldsymbol{B}\left(\delta\hat{\boldsymbol{d}}^{*\mathrm{e}}\right)$. The discretized formulation of (33) can be written by inserting these equations as follows:

$$\sum_{\mathrm{e}=1}^{n_{\mathrm{ele}}} \left\{ \left(\delta\hat{\boldsymbol{d}}^{*\mathrm{e}}\right)^{\mathrm{T}} \int_{\mathrm{Y_e}} \boldsymbol{B}^{\mathrm{T}} \mathbb{C} \boldsymbol{B} \mathrm{d}y \left(\hat{\boldsymbol{w}}^{\mathrm{e}}\right) \right\} = 0. \tag{38}$$

As the virtual fluctuation displacement $\delta\hat{\boldsymbol{d}}^{*\mathrm{e}}$ is arbitrary, the discretized formulation of (33) is expressed by assembling (38) over the unit cell as:

$$\boldsymbol{K}^{\mathrm{m}}\hat{\boldsymbol{w}} = \boldsymbol{0} \qquad \text{with} \qquad \boldsymbol{K}^{\mathrm{m}} = \sum_{\mathrm{e}=1}^{n_{\mathrm{ele}}} \int_{\mathrm{Y_e}} \boldsymbol{B}^{\mathrm{T}} \mathbb{C} \boldsymbol{B} \mathrm{d}y, \tag{39}$$

where $\boldsymbol{K}^{\mathrm{m}}$ is the global stiffness matrix of a unit cell and $\hat{\boldsymbol{w}}$ is the global nodal micro-displacement vector.

At this stage the boundary conditions (12) and (13) have not been included in (39) yet. In order to establish the extended micro-scale BVP aforementioned, the relative displacement q is embedded to (39) as constraints by replacing pairs of DOFs in $\hat{\boldsymbol{w}}$. For this purpose, each external material point is also 'discretized' to an element with a single node which has two DOFs and no mass. Since the external material points enable us to control the components of the macro-scale stress and deformation, as explained above, the node corresponding to an external material point is referred to as a *control node* in this study. Thus, we obtain an *extended system* of FE-discretized equations involving four additional DOFs of two control nodes. In the following, we introduce some specific usages of the two control nodes to solve the extended system.

First, the macro-scale strain is assumed to be known; that is, all the components of the macro-strain $\boldsymbol{E}$ are given as data. Using (13), we obtain all the components of the nodal relative displacement vector $q^{[k]}$ at the two control nodes. Then, given all the components $q_i^{[k]}$, we solve the extended system of FE equations with the appropriate number of 'two-point' constraints realized by (12).

This procedure starts from applying a transformation matrix $\boldsymbol{\Phi}$ such as,

$$\tilde{\boldsymbol{w}} = \boldsymbol{\Phi}\hat{\boldsymbol{w}}, \tag{40}$$

where $\boldsymbol{\Phi}$ is an operator which transforms $\hat{\boldsymbol{w}}$ to $\tilde{\boldsymbol{w}}$ and $\tilde{\boldsymbol{w}}$ is the nodal displacement vector in which some components are replaced by the components of $\boldsymbol{q}^{[k]}$. For example, concentrating only on $\boldsymbol{q}^{[1]}$, we impose the corresponding two points on the boundaries $\partial Y^{[-1]}$ and $\partial Y^{[1]}$ whose DOFs are defined as (w_a, w_b) and (w_c, w_d), respectively, to be periodically constrained. Then, we can establish $\tilde{\boldsymbol{w}}$ from $\hat{\boldsymbol{w}}$ as shown in Fig. 3, namely

$$\hat{\boldsymbol{w}} = \left\{ w_1 \quad w_2, \ldots, w_a \quad w_b, \ldots, w_c \quad w_d, \ldots, w_N \right\} \tag{41}$$

and

$$\tilde{\boldsymbol{w}} = \left\{ w_1 \quad w_2, \ldots, w_a \quad w_b, \ldots, q_1^{[1]} \quad q_2^{[1]}, \ldots, w_N \right\} \tag{42}$$

$$\text{with} \qquad w_c - w_a = q_1^{[1]} \quad \text{and} \quad w_d - w_b = q_2^{[1]}. \tag{43}$$

where N is the total number of DOFs in the unit cell without the number of DOFs of the external material points. Of course, as the above example is simply for one set of the constrained points on the $\partial Y^{[-1]}$ and $\partial Y^{[1]}$, all other constrained points have to be considered in $\tilde{\boldsymbol{w}}$ at the same time. Note that one set of $\boldsymbol{q}^{[k]}(k = 1 \text{ or } 2)$ can control all constrained points staying on $\partial Y^{[-k]}$ and $\partial Y^{[k]}$, see again Fig. 3.

Then, inserting (40) into (39) and pre-multiplying the operator $\boldsymbol{\Phi}$ by both sides of (39) yields,

$$\tilde{\boldsymbol{K}}^{\mathrm{m}}\tilde{\boldsymbol{w}} = \boldsymbol{0} \quad \text{with} \quad \tilde{\boldsymbol{K}}^{\mathrm{m}} = \boldsymbol{\Phi}\boldsymbol{K}^{\mathrm{m}}\boldsymbol{\Phi}^{\mathrm{T}}. \tag{44}$$

This linear equations can be condensed depending on the distribution of components of $\boldsymbol{q}^{[k]}$ in $\tilde{\boldsymbol{w}}$. After solving this linear equation, unknown components in $\tilde{\boldsymbol{w}}$ are determined. The results of the FEA contain not only the micro-scale displacement $\tilde{\boldsymbol{w}}$, strain $\boldsymbol{\varepsilon}$ and stress $\boldsymbol{\sigma}$, but also the reaction force $\boldsymbol{R}^{[k]}$ as aforementioned. This means that $\boldsymbol{R}^{[k]}$ can be obtained by (15) since the traction force vector $\boldsymbol{t}^{[k]}$ on $\partial Y^{[k]}$ is obtained by the Cauchy law $\boldsymbol{t}^{[k]} = \boldsymbol{\sigma} e_k$. Therefore, the macro-stress Σ_{jk} can be computed from (16), without performing a numerical integration on (1). Finally, as shown in (19), the macro-material stiffness $\mathbb{C}^{\mathrm{H}}$ can be obtained by computing the macro-stress Σ_{jk} separately three times according to the corresponding relative displacements.

References

Amstutz S, Giusti SM, Novotny AA, de Souza NEA (2010) Topological derivative for multi-scale linear elasticity models applied to the synthesis of microstrucures. Int J Num Meth Eng 84:733–756

Bendsøe MP, Sigmund O (1999) Material interpolation schemes in topology optimization. Achieve Appl Mech 69:635–654

Bendsøe MP, Sigmund O (2003) Topology optimization, theory, method and applications. Springer-Verlag, Berlin

Diaz A, Sigmund O (1995) Checkerboard patterns in layout optimization. Struct Multidisc Optim 10(1):40–45

Feyel F, Chaboche JL (2000) FE^2 multiscale approach for modelling the elastoviscoplastic behaviour of long fibre SiC/Ti composite materials. Comput Methods Appl Mech Eng 183:309–330

Jog CS, Haber RB (1996) Stability of finite element models for distributed-parameter optimization and topology design. Comput Methods Appl Mech Eng 130:203–226

Kato J, Lipka A, Ramm E (2009) Multiphase material optimization for fiber reinforced composites with strain softening. Struct Multidisc Optim 39:63–81

Larsen UD, Sigmund O, Bouwstra S (1997) Design and fabrication of compliant micromechanisms and structures with negative Poisson's ratio. J MEMS 6(2):99–106

Niu B, Yan J, Chen G (2009) Optimum structure with homogeneous optimum cellular material for maximum fundamental frequency. Struct Multidisc Optim 39(2):115–132

Patnaik SN, Guptill JD, Berke L (1995) Merits and limitations of optimality criteria method for structural optimization. Int J Num Meth Eng 38:3087–3120

Rodrigues H, Guedes JM, Bendsøe MP (2002) Hierarchical optimization of material and structure. Struct Multidisc Optim 24:1–10

Sigmund O (1994) Materials with prescribed constitutive parameters: an inverse homogenization problem. Int J Solid Struct 31(13):2313–2329

Sigmund O (2007) Morphology-based black and white filters for topology optimization. Struct Multidisc Optim 33:401–424

Sigmund O, Torquato S (1997) Design of materials with extreme thermal expansion using a three-phase topology optimization method. J Mech Phys Solids 45(6):1037–1067

Sigmund O, Pettersson J (1998) Numerical instabilities in topology optimization: a survey on procedures dealing with checkerboards, mesh-dependencies and local minima. Struct Multidisc Optim 16(1):68–75

Smit RJM, Brekelmans WAM, Meijer HEH (1998) Prediction of the mechanical behavior of nonlinear heterogeneous systems by multi-level finite element modeling. Comput Methods Appl Mech Eng 155:181–192

Su W, Liu S (2010) Size-dependent optimal microstructure design based on couple-stress theory. Struct Multidisc Optim 42(2):243–254

Terada K, Kikuchi N (2001) A class of general algorithms for multi-scale analyses of heterogeneous media. Comput Methods Appl Mech Eng 190:5427–5464

Terada K, Inugai T, Hamana Y, Miyori A, Hirayama N (2008) Parameter identification for anisotropic hyperelastic materials by numerical material testing. Trans JSCES 13(1):513–516. (in Japanese)

Terada K, Kato J, Hirayama N, Inugai N, Yamamoto K (2013) A method of two-scale analysis with micro-macro decoupling scheme: application to hyperelastic composite materials. Comput Mech. doi:10.1007/s00466-013-0872-5

Watanabe I, Terada K (2010) A method of predicting macroscopic yield strength of polycrystalline metals subjected to plastic forming by micro-macro de-coupling scheme. Int J Mech Sci 52(2):343–355

Wieckowski Z (2000) Dual finite element methods in homogenization for elastic-plastic fibrous composite material. Int J Plast 16:199–221

Zheng SF, Ding K, Denda M, Weng GJ (2000) A dual homogenization and finite-element study on the in-plane local and global behavior of a nonlinear coated fiber composite. Comput Methods Appl Mech Eng 183:141–155

Zhou M, Rozvany GIN (1991) The COC algorithm, part II : topological, geometrical and generalized shape optimization. Comp Meths Appl Mech Eng 89:309–336